Effect of Benzoic Acid as a Modulator in the Structure of UiO-66: An Experimental and Computational Study

Cesare Atzori,[†] Greig C. Shearer,[‡] Lorenzo Maschio,[§] Bartolomeo Civalleri,[§] Francesca Bonino,[†] Carlo Lamberti,[§,‖] Stian Svelle,[‡] Karl Petter Lillerud,[‡] and Silvia Bordiga*,[†,‡]

[†]Department of Chemistry, NIS and INSTM Reference Centre, University of Turin, Via Quarello 15, I-10135 Turin, Italy
[‡]Department of Chemistry, University of Oslo, P.O. Box 1033, N-0315 Oslo, Norway
[§]Department of Chemistry, NIS and INSTM Reference Centre, University of Turin, Via Giuria 7, I-10125 Turin, Italy
[‖]IRC "Smart Materials", Southern Federal University, Zorge Street 5, 344090 Rostov-on-Don, Russia

Ⓢ Supporting Information

ABSTRACT: The identification and quantification of defects are undoubtedly thorough challenges in the characterization of "defect-engineered" metal−organic frameworks (MOFs). UiO-66, known for its exceptional stability and defect tolerance, has been a popular target for defect-engineering studies. Herein, we show that synthesizing UiO-66 in the presence of an excess of benzoic acid is a reliable method for obtaining UiO-66 samples with a very high concentration of missing-cluster defects, allowing one to modulate specific properties (i.e., surface area and hydrophobicity). This was elucidated by a multitechnique marriage of experimental and computational methods: a combination of PXRD, dissolution/^{1}H NMR spectroscopy, and N_2 sorption measurements was used to quantify the defect loading, while vibrational spectroscopies (FTIR and Raman) allowed us to unequivocally identify the defect structure by comparison with DFT-simulated spectra and visual analysis of the computed vibrational modes.
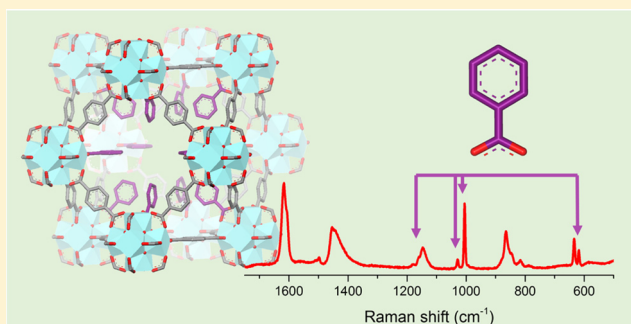
1. INTRODUCTION

Among the numerous classes of porous materials, metal−organic frameworks (MOFs) stand out for their structural and chemical diversity, exhibiting a wide range of well-defined pore size distributions and chemical functionalities.[1,2] This variety endows MOFs with incredible potential in many areas of technological relevance, e.g., adsorption[3] and catalysis,[4] but their real-world applicability in these areas has thus far been hindered by serious drawbacks, such as poor stability, particularly to moisture.[5−9] Much attention has therefore been given to relatively stable subclasses of MOFs, e.g., zirconium(IV) MOFs, particularly those with clusters based on a Zr_6 octahedral core.[10−15] The most widely studied material among these "Zr_6 MOFs" is UiO-66 (Figure 1), in which the Zr_6-oxyhydroxide clusters are 12-fold connected by 1,4-benzenedicarboxylate (BDC, a linear ditopic linker), resulting in a highly symmetric face-centered cubic (fcu) structure.[12]

While UiO-66 is indeed exceptionally thermally, chemically, and mechanically stable, its performance in commonly proposed applications (e.g., adsorption, separation, and catalysis) is limited by its relatively modest porosity and lack of chemical functionality. In recognition of these shortcomings, many researchers have opted to instead focus on isoreticularly expanded and/or functionalized UiO-66 derivatives (e.g., UiO-67, UiO-66-NH$_2$), which offer improvements in these

areas.[16−33] However, these derivatives generally harbor two rather significant drawbacks with respect to UiO-66: lower stability[18,21,23,24,34,35] and higher cost. The bulk of their expense can be attributed to the functionalized and/or extended organic linker(s), many of which are not even commercially available, necessitating the development of in-house synthesis procedures,[36] which can take months (or longer) to optimize unless the molecule has already been reported in the literature. It is therefore clear that an alternative approach for tuning the porosity and functionality of UiO-66 (and thus, performance) is desired.

One such alternative approach is "defect engineering", a term often used as shorthand for the practice of manipulating defects via controlled, synthetic means.[37−46] This approach has proven to be particularly effective for UiO-66,[16,37,38,43−72] which is famed for its ability to tolerate an extraordinarily high concentration of defects while retaining much of its stability[37] [except for certain cases where the thermal stability has been shown to be heavily compromised[73] and one sample (50Benz-HA in ref 49) that was found to have reduced water stability]. We stress that this fascinating trait is not just an academic
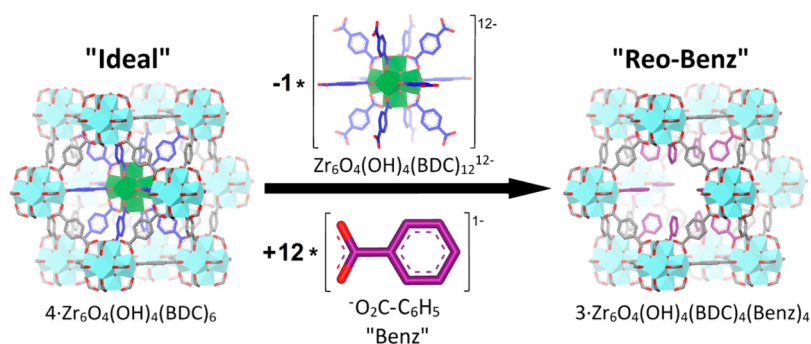
Figure 1. Illustration showing how the structure of a "Reo-Benz" defect differs from that of ideal, defect-free UiO-66. Hydrogen atoms have been omitted for the sake of clarity.

curiosity; many studies have shown that defects significantly enhance UiO-66's porosity (see refs 37, 38, 43, 44, 46, 48, 49, 53, 58, 59, 61, 73, and 74) and reactivity (see refs 44, 47, 49, 50, 57, 60, and 62), leading to better performances in a wide variety of applications (see refs 38, 48−50, 53, 56−59, 62−67, 75, and 76). Such positive demonstrations have encouraged many researchers to seek out strategies to gain synthetic control over the defects in the UiO-66 framework.

To this end, the most common method is to synthesize UiO-66 in the presence of additives known as "modulators".[68,69,77−80] Many types of modulator (e.g., HCl,[61,63] HF,[68] NH$_4$OH,[79] and amino acids[69]) are known to promote the formation of defects, but monocarboxylic acid "coordination modulators" (e.g., acetic acid, formic acid, benzoic acid, etc.) are the most widely studied and, thus, best understood.[37,38,46−50,52−55,58,59,77] In recent work,[37,49] we proved that monocarboxylic acid modulation promotes the formation of "missing-cluster defects" whose charge and coordination deficiencies are compensated by modulator ligands (in their carboxylate form; see benzoate ligands in Figure 1). More importantly, we showed that these defects can massively enhance the porosity and reactivity of the material[49,73] and that new, otherwise elusive functionalities can be incorporated by postsynthetically exchanging the defect-compensating ligands.[49]

Another important (albeit less striking) aspect of our systematic investigations is that they have enabled us to objectively compare different monocarboxylic acid modulators for their propensity for introducing defects to the UiO-66 framework, a property which we hereafter refer to as their "defect-inducing potency". On the basis of such comparisons, we have identified trifluoroacetic acid[37] and benzoic acid[49] as the most potent modulators we have investigated thus far, and have ascribed their effectiveness to a combination of acidity,[37] solubility,[49] and steric[49] effects. While the defect-inducing potency of the two modulators are roughly equivalent, we now harbor a strong preference toward benzoic acid for the following reasons: (1) Trifluoroacetic acid (a strong acid) readily catalyzes the hydrolysis of DMF during UiO-66 synthesis, generating formic acid which then goes on to act as a modulator in its own right, resulting in a material with defects compensated by a combination of trifluoroacetate and formate ligands.[37] This increases the complexity and heterogeneity of the material in a manner that is probably not entirely reproducible, and is much less of an issue when benzoic acid (a much weaker acid) is employed as the modulator.[49] (2) Trifluoroacetic acid (bp = 72.4 °C) is a relatively volatile molecule that may therefore evaporate from the solution during UiO-66 syntheses. We speculate that this volatilization could occur to different extents and rates from one synthesis batch to the next, potentially affecting reproducibility, a situation that is completely avoided by using the nonvolatile benzoic acid (bp = 249.2 °C) as the modulator. (3) In our experience, UiO-66 syntheses modulated by trifluoroacetic acid often provide poor yields, a negative outcome which is much less severe when benzoic acid is employed as the modulator. (4) Trifluoroacetic acid-modulated syntheses tend to yield UiO-66 samples with very poorly defined crystal morphology and size,[37,50] while benzoic acid-modulated syntheses provide reasonably monodisperse octahedral crystals.[20,49,59,77] (5) Benzoic acid is much cheaper than trifluoroacetic acid.

It is important to keep in mind that all of the findings discussed thus far were backed up by a large amount of convincing experimental evidence, something that we feel is especially vital for defect-engineering pursuits, since disorder is notoriously challenging to characterize. In acknowledgment of this challenge, researchers have sought to develop methods that are able to detect, quantify, and evaluate the nature of the defects in different UiO-66 samples, preferably with routine characterization techniques available in most laboratories. To this end, most research groups (including our own) employ some combination of PXRD (see refs 37, 49, 52, 54, and 73), TGA (see refs 37, 49, 50, 53−55, 58, 61, 68, 69, and 73), dissolution/^{1}H NMR spectroscopy (see refs 37, 47, 49, 53, 59, and 69), and N$_2$ adsorption measurements (see refs 37, 38, 47−49, 53, 58, 59, 61, 63, 68, 69, and 73) [sometimes in conjunction with simulations (see refs 37, 49, 61, 67, and 73)]. While indirect, this approach has proven to be valuable for detecting defects and assessing their concentration via simple semiquantitative data analysis methods.[37,49] Conversely, vibrational spectroscopies (FTIR, Raman) have thus far had only a peripheral, qualitative role for characterizing the defectivity of UiO-66. For example, they have been used to detect the presence of different defect-compensating ligands (i.e., deprotonated modulator molecules[37,49]) and superfluous hydroxyl groups[81,82] (also thought to terminate defects in some cases[57,60,61,65,70−72]) and to indicate defectivity by noting differences between experimental spectra and that simulated from the ideal, defect-free UiO-66 structural model.[73] This rather limited use is somewhat surprising given that vibrational spectroscopies are traditionally very well suited to characterize defects,[83,84] and it was this realization that motivated us to investigate these techniques further herein.

To this end, we synthesized a series of five defective UiO-66 samples, each obtained in the presence of different amounts of benzoic acid (our preferred defect-engineering modulator; see reasons above). All of the samples (given the general name

"*x*Benz", where *x* is the molar equivalents of benzoic acid used in the synthesis, with respect to $ZrCl_4$) were then characterized by means of Raman and FTIR spectroscopies, as well as the methods more commonly used for characterizing defects in UiO-66 (PXRD, dissolution/^{1}H NMR, and nitrogen sorption measurements). In accordance with our previous studies,[37,49] the results show that (1) using benzoic acid as a modulator yields UiO-66 samples with a high concentration of missing-cluster defects with benzoate as the compensating ligand [herein named "Reo-Benz" defects (see Figure 1) due to their RCSR[85]-denoted topology (reo)] and (2) the concentration of these defects systematically increases as increasing amounts of benzoic acid are used in the synthesis. Although we are fully convinced of these conclusions, we speculate that some of the MOF community may still be skeptical due to the indirect manner in which these methods probe defectivity. This potential criticism is opposed by the vibrational spectroscopy results, which, when compared with simulated spectra, provide direct and unequivocal evidence for these conclusions (and those of our previous studies[37,49]). Perhaps more importantly, this paper demonstrates that vibrational spectroscopies can be a powerful tool for characterizing defects in MOFs, especially when experimental results are compared with spectra simulated from models of proposed defect structures.[86,87]

2. EXPERIMENTAL SECTION

2.1. Materials Synthesis. *2.1.1. Defective UiO-66 Samples.* The five defective UiO-66 samples (named 10Benz, 20Benz, 30Benz, 40Benz, and 50Benz) were synthesized by the same method, albeit with different amounts of benzoic acid as a modulator (see Table 1). First, the synthesis solutions were

Table 1. Quantities of Benzoic Acid Used in the Synthesis of the Five Defective UiO-66 Samples

sample[a]	amount of benzoic acid used in synthesis
10Benz	8.807 g (72.12 mmol)
20Benz	17.613 g (144.23 mmol)
30Benz	26.420 g (216.34 mmol)
40Benz	35.226 g (288.45 mmol)
50Benz	44.033 g (360.57 mmol)

[a]The names of the samples are derived from the benzoic acid:$ZrCl_4$ molar ratio in their respective synthesis solutions.

prepared by sequentially adding 1.680 g of $ZrCl_4$ (7.209 mmol), 0.173 mL of H_2O (9.603 mmol), benzoic acid (quantities given in Table 1), and 1.198 g of 1,4-benzenedicarboxylic acid (H_2BDC, 7.211 mmol) to a 1 L Erlenmeyer flask containing 413.2 mL of warm (ca. 70 °C) *N,N′*-dimethylformamide (DMF, 5336 mmol) under constant magnetic stirring.

Once the reagents had fully dissolved, the stirring bars were removed and watch glasses were placed over the mouths of the flasks as a loose cover. The covered synthesis solutions were then placed in an oven preheated to 120 °C and were allowed to react over a period of 24 h before applying the purification steps given in section 2.1.3.

2.1.2. "Defect-Free" UiO-66 (Ref.). The "defect-free" UiO-66 sample (Ref.) was synthesized via an optimized version[37,49] of a procedure originally outlined by Serre and co-workers[88] and later promoted by us.[73] First, the synthesis mixture was prepared by sequentially dissolving 3.781 g of $ZrCl_4$ (16.22 mmol), 2.865 mL of 35% HCl (32.45 mmol), and 5.391 g of H_2BDC (32.45 mmol) in 97.40 mL of warm (ca. 70 °C) *N,N′*-

dimethylformamide (DMF, 1258 mmol) under constant magnetic stirring. Once all reagents had fully dissolved, the mixture was transferred to a 200 mL Teflon liner, sealed in a stainless steel autoclave, and placed in an oven preheated to 220 °C. After 24 h of reaction at this temperature, the autoclave was removed from the oven and rapidly cooled by dropping it into a bucket of cold tap water for 30 min before applying the purification steps given in section 2.1.3.

2.1.3. Purification Procedures. After all reactions, the resulting microcrystalline powder precipitates were separated from their synthesis solutions via centrifugation and washed by shaking them overnight in 80 mL of fresh DMF. Three further separation/washing cycles were performed the next day, albeit for a shorter duration (ca. 2 h per wash) before the washed products were separated by centrifugation, dried overnight in an oven set to 60 °C, and ground with a mortar and pestle. The samples were then subjected to a further "activation" procedure to remove the DMF guest molecules from their pores. This was achieved by heating them at 200 °C for 24 h in a conventional oven, a simple treatment which we have found to be very effective for UiO-66.[37,49] The Ref. sample was subjected to a further heat treatment (dubbed "calcination"), in which unidentified nonvolatile organic impurities[37] are removed via a two-step program on a multistep muffle furnace. In the first step, a 5 °C min^{−1} ramp was used to heat the material from room temperature to 200 °C, at which it was held for 10 min. A 0.5 °C min^{−1} ramp was then used between 200 and 270 °C, where the temperature was held for 70 h. After calcination, the product was allowed to cool to room temperature naturally.

The activated/calcined samples are not completely empty, as they adsorb a small amount of atmospheric water vapor when allowed to cool to room temperature in air. The theoretical yields of the procedures (discounting adsorbed water) is 2 g for the defective samples and 4.5 g for the defect-free one.

2.2. Experimental Methods. *2.2.1. Powder X-ray Diffraction (PXRD).* Samples were prepared for measurement by dispersing 30 mg of sample on a flat, glass plate PXRD sample holder with a diameter of 2.5 cm. A stretched piece of plastic film was then used to spread, flatten, and hold the sample in position for measurement. The plastic film is evident in the PXRD patterns, appearing as two broad peaks covering 2θ ranges of ca. 20°–22° and 23°–24°.

PXRD patterns (Cu Kα radiation, $\lambda = 1.5418$ Å, 2θ range = 2°–50°, time scale = 1, resulting in a *d*-spacing down to 1.82 Å) were collected in reflectance Bragg−Brentano geometry with a Bruker D8 Discovery diffractometer equipped with a focusing Ge-monochromator and a Bruker LYNXEYE detector.

Values of the relative intensity of the broad peak [$Rel(I)_{BP}$] have been extracted from the patterns by fitting with a peak-shaped function (a pseudo-Voigt or a Pearson VII, depending on which one gave the lowest error) and normalizing the area of the fitted peak by dividing by the intensity (measured in the same manner of the broad one) of three key reflections [the (100), (200) and (600)] of UiO-66. A detailed description of this method can be found in section 4 of the Supporting Information of the present paper and in two preceding works.[37,49]

2.2.2. Dissolution/^{1}H NMR Spectroscopy. Samples were prepared by weighing 20 mg of the MOF sample of interest into an NMR tube and adding 600 μL of 1 M NaOH (in D_2O). The NMR tube was then capped and the contents were mixed by inverting the tube two or three times. The MOF was then left to digest over a period of 24 h before measurement. This

hydroxide-based procedure dissolves only the organic portion of the MOF (linker, modulator, solvent etc.), while the inorganic content is converted into ZrO_2, which sinks to the bottom of the NMR tube and does not influence the spectra. Liquid ^1H NMR spectra were obtained with a Bruker Avance DPX-300 NMR Spectrometer (300 MHz). The relaxation delay (d1) was set to 20 s to improve the reliability of integration and, thus, the accuracy of the molar ratios determined from the results. The number of scans (ns) was 64. Molar ratios were extracted from these spectral data using a procedure reported in section 6 of the the Supporting Information of the present paper and two preceding works.[37,49]

2.2.3. Nitrogen Sorption Measurements at 77 K. Nitrogen sorption measurements were performed on a BelSorp mini II instrument at 77 K. In each experiment, approximately 50 mg of the sample of interest was weighed into a 9.001 cm^3 glass cell. Prior to measurement, guest molecules were removed from the MOF pores via simultaneous vacuum and heat treatment, first for 1 h at 80 °C and then for 2 h at 200 °C. The sample cells were then immersed in a Dewar of liquid nitrogen for the duration of the nitrogen adsorption measurement. BET areas were extracted from the nitrogen adsorption isotherms via the method described in section 5 of the Supporting Information of the present work and in two of our previous papers.[37,49]

2.2.4. Attenuated Total Reflection Infrared (ATR-IR) Spectroscopy. Loose MOF powder was introduced into a Bruker Vertex70 FTIR spectrometer equipped with a Bruker OPTIK Platinum ATR accessory with a diamond internal reflection element. ATR-IR spectra (2 cm^{-1} resolution, 256 scans) were then recorded in the 4000−600 cm^{-1} range and detected with an MCT detector. The spectral intensity was corrected for the change in the effective thickness value as a function of the incident wavelength.

2.2.5. Transmission IR Spectroscopy. Samples were measured in the form of small (ca. 2 cm^2), thin, self-supporting wafers, which were prepared by pellet-pressing ca. 30 mg of pure, undiluted MOF powder with a force of ca. 10 kN. In separate experiments, wafers were placed in a home-built airtight quartz cell with mid-IR transparent KBr windows. Before measurement, guest molecules were removed from the MOF pores by attaching the quartz cell to a custom-made vacuum line and applying simultaneous vacuum and heat treatment (1 h at 80 °C and then 2 h at 200 °C). The transmission FTIR spectra were then recorded in the 4000−600 cm^{-1} range with a Bruker Vertex 70 FTIR spectrometer equipped with a MCT detector (2 cm^{-1} resolution, 32 scans).

2.2.6. Raman Spectroscopy. Samples were prepared and pretreated in the same manner as for the transmission FTIR measurements, albeit using another type of locally constructed airtight cell featuring a Suprasil quartz cuvette. Raman spectra were recorded over a wavenumber range of 1800−500 cm^{-1} on a Renishaw inVia Raman microscope spectrometer in back-scattering mode. A 785 nm diode laser was used for the excitation, and the scattered photons were dispersed by a 1200 lines/mm grating monochromator and collected on a CCD camera whose collection optic was set at 20× objective summing up 66 scans with an exposition time of 20 s per step.

2.3. Computational Methods. *2.3.1. Used Models.* Two atomistic models were used for both DFT calculations and isotherm simulations: the crystallographic structure of UiO-66[12,82] for the defect-free model (named "Ideal") and a defective benzoate-containing structure (dubbed "Reo-Benz") that was created by starting from the perfect UiO-66

framework. First, from the primitive unit cell of UiO-66 {114 atoms, $Zr_6O_4(OH)_4[C_6H_4(COO)_2]_6$} the crystallographic cubic cell was built that corresponds to a 4 times larger supercell (456 atoms). Then, to create the defect, a $Zr_6O_4(OH)_4$ unit was removed along with the carboxylate groups of the neighboring linkers, and finally, the dangling bonds on the aromatic rings were saturated with hydrogen atoms. The resulting structure was comprised of a 414-atom cubic unit cell {$3Zr_6O_4(OH)_4[C_6H_4(COO)_2]_4[C_6H_5COO]_4$} that has 12 benzoic moieties in the defective site, as shown in Figure 1.

2.3.2. DFT Calculations. All calculations were performed by means of the CRYSTAL14 ab initio code.[89] The hybrid B3LYP[90,91] method, combined with an all-electron Gaussian basis set, was employed. The basis set consists of the following contractions of Gaussian functions: (8s)-(7631sp)-(621d) for Zr, (8s)-(411sp)-(1d) for O, (6s)-(31sp)-(1d) for C, and (31s)-(1p) for H (see ref 82 for details). All computational parameters were the same as in the previous work of Valenzano et al.,[82] except for the shrinking factor used in reciprocal space sampling (here raised to 3 from the original value of 2). Both the perfect (Ideal) and defective (Reo-Benz) UiO-66 models were fully relaxed by keeping the symmetry of the systems (24 symmetry operators). The presence of the defect leads to a negligible expansion of the unit cell volume (i.e., less than +0.1%), which is probably due to the well-known rigidity of the UiO-66 framework. Vibrational frequencies were computed at the Γ point on the optimized geometries.[92] Infrared and Raman intensities were calculated via an entirely analytical procedure based on a linear response.[93,94] A Lorentzian broadening of 5 cm^{-1} was adopted for both the infrared and Raman spectra. Vibrational frequencies were shifted by a factor of 0.98 in order to compensate for the well-known DFT overestimation effect.

The choice of the B3LYP functional is justified by consistency with previous works on the UiO-66 crystal. The introduction of empirical dispersion corrections (Grimme's D3 with three-body contribution) leads to a mild contraction of cell volumes (1.4% for the perfect structure, less than 2% for the defective one), resulting in shifts for the individual frequencies not larger than 10 cm^{-1}. Since the discussion in the following focuses on isolated features of the vibrational spectra relative to the benzoate defect rather than collective modes, we consider the choice of the functional of minor importance.

2.3.3. Isotherm Simulation. Adsorption isotherms were simulated with the "adsorption isotherm" task within the "Sorption Tools" menu in Accelrys Materials Studio version 8.1. The simulations were performed at 77 K, using a geometry-optimized N_2 molecule as the adsorptive and a single, geometry-optimized unit cell of the model structure of interest as the adsorbent. We adopted the Metropolis method and the COMPASS force field. The isotherms were simulated over a pressure range of 0.01−100 kPa, in which 50 fugacity steps were distributed logarithmically in order to increase the number of data points in the steep initial portion of the isotherm. The "Fine" quality setting was used for all simulations. Charges were force field assigned, while electrostatic forces were calculated with the Ewald method. The "atom-based" method was adopted for the calculation of van der Waals forces. No constraints were assigned.

3. RESULTS AND DISCUSSION

Figure 2 illustrates the complete set of PXRD patterns obtained on the full series of samples over a 2θ range of $2°-35°$. All the
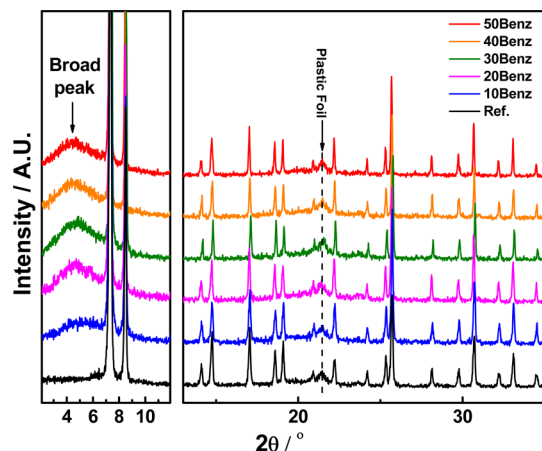
Figure 2. PXRD patterns obtained on the six UiO-66 samples. The same y-scale is applied to both plots.

samples are highly crystalline and with the expected patterns, except for the region preceding the first reflection of the UiO-66 phase. This region is emphasized in the left plot of Figure 2, where it can be seen that a very broad peak (spanning a 2θ range of ca. $2°-7°$) is observed in the PXRD patterns obtained on the samples synthesized in the presence of benzoic acid. In a couple of previous works[37,49] we unambiguously assigned this "broad peak" to very tiny "nanoregions" of missing cluster defects and showed that the relative intensity of the broad peak [$Rel(I)_{BP}$] is correlated with the concentration of these defects. The absence of this peak in the pattern obtained on the reference UiO-66 sample ("Ref.", black line in Figure 2) proves its very low defectivity. In contrast, the broad peak is already clearly present in the pattern obtained on 10Benz, and its intensity (and, thus, the concentration of missing cluster defects) systematically increases in 20Benz and 30Benz, at which point it essentially plateaus. This is more visually and quantitatively evident in Figure 3, where the $Rel(I)_{BP}$ values (calculated via the method outlined in section 4 of the Supporting Information; see Table 2 and Table S1 for
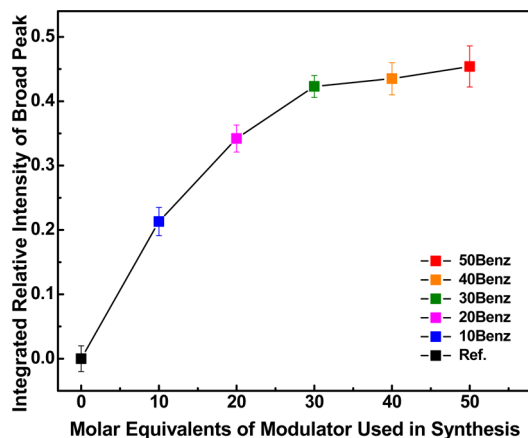
Figure 3. Integrated relative intensity of the broad diffraction peak [$Rel(I)BP$], (see Table 2 and Table S1) vs the molar equivalents of benzoic acid added to the UiO-66 synthesis mixture.

Table 2. Summary of the Quantitative Experimental Data Extracted from the PXRD, Dissolution/^{1}H NMR, and Nitrogen Adsorption, Results Obtained on the UiO-66 Samples, and Theoretical Values from the Models (see Figure 1)

sample	$Rel(I)_{BP}$/error	$\dfrac{n_{mod.}}{n_{BDC}}$	BET area $(m^2 g^{-1})$	ref
Ref.	0.000/0.020	0.00	1236	37
10Benz	0.213/0.022	0.34	1252	this work
20Benz	0.342/0.021	0.59	1382	this work
30Benz	0.423/0.017	0.69	1480	this work
40Benz	0.435/0.025	0.78	1494	this work
50Benz	0.454/0.032	0.79	1515	this work

model	$Rel(I)_{BP}$/error	$\dfrac{n_{mod.}}{n_{BDC}}$	BET area $(m^2 g^{-1})^a$	ref
Ideal	–	0.00^b	1241	37
Reo-Benz	–	1.00^c	1532	49

^{a}Calculated from the simulated nitrogen adsorption isotherms (see Figure 6a). ^{b}There are no monocarboxylate ligands in the ideal UiO-66 composition, $Zr_6O_4(OH)_4(BDC)_6$, so $\frac{n_{mod.}}{n_{BDC}} = 0$. ^{c}The composition of Reo-Benz is $Zr_6O_4(OH)_4(BDC)_4(Benz)_4$, where "Benz" is benzoate, a monocarboxylate ligand. Thus, $\frac{n_{mod.}}{n_{BDC}} = \frac{4}{4} = 1$.

numerical data) are plotted against the molar equivalents of benzoic acid used in the MOF syntheses. These observations suggest that benzoic acid is very effective at creating missing-cluster defects in UiO-66, even at relatively low concentrations.

Liquid ^{1}H NMR spectroscopy was used to identify and determine the molar ratios between the organic components in the UiO-66 samples. Figure 4 compares the dissolution/^{1}H
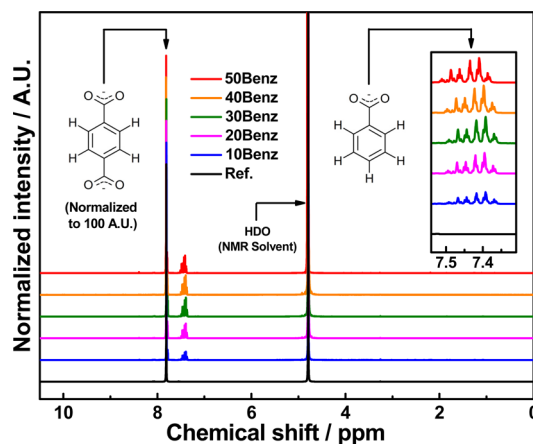

Figure 4. Dissolution/^{1}H NMR spectra obtained on the six UiO-66 samples.

NMR spectra obtained on all six samples and clearly illustrates the appearance of signals attributed to benzoate in the samples synthesized in the presence of benzoic acid. Since benzoate ligands are thought to terminate the missing cluster defects in these materials, their benzoate content is essentially a measure of their defectivity. However, differences in the intensity of the benzoate signal throughout the series are not particularly apparent upon visual inspection of the spectra, making it difficult to discern qualitative trends in their benzoate content by observation alone.

Regardless, the real strength of the dissolution/^{1}H NMR is that one can quantify the molar ratios between the organic components in MOF samples by integrating the spectra and

performing simple calculations. Thus, we determined the benzoate/BDC molar ratios $\left(\frac{n_{\text{Benz}}}{n_{\text{BDC}}}\right)$ in our samples, which can be considered as a quantitative descriptor for their benzoate content. Moreover, a very small concentration of formate moieties (originating from the in situ hydrolysis of DMF during the MOF synthesis[37]) was determined via integration of the faint signal falling at ca. 8.4 ppm, yielding the formate to BDC molar ratio $\left(\frac{n_{\text{Form.}}}{n_{\text{BDC}}}\right)$. This contribution was added to $\frac{n_{\text{Benz}}}{n_{\text{BDC}}}$ to get the "total modulator to BDC molar ratio" $\left(\frac{n_{\text{mod.}}}{n_{\text{BDC}}}\right)$, which is a quantitative descriptor for the amount of monocarboxylate ligands in the samples (and, thus, the concentration of defects in the UiO-66 framework[37]). These calculations were somewhat complicated by the overlap of the BDC and benzoate signals, as discussed in section 6 of the Supporting Information, where full details of the method are provided.
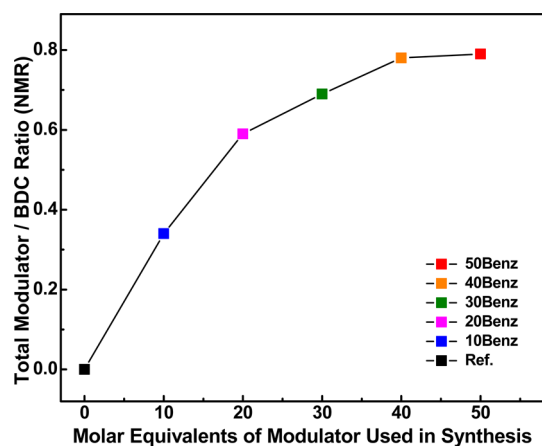

Figure 5. Graph obtained when the total modulator to BDC molar ratios $\left(\frac{n_{\text{mod.}}}{n_{\text{BDC}}}\right)$ (see Table 2 and Table S2 of the Supporting Information) are plotted against the molar equivalents of modulator (benzoic acid) added to the UiO-66 synthesis mixture.

Figure 5 is the plot obtained when the $\frac{n_{\text{mod.}}}{n_{\text{BDC}}}$ values of the six samples (see Table 2 and Table S2 of the Supporting Information for the numerical data) are plotted against the molar equivalents of benzoic acid added to their syntheses. The plot clearly shows that the extent of monocarboxylate incorporation (and, thus, the defectivity of the samples) systematically increases throughout the series but essentially plateaus for the last two samples (40Benz and 50Benz). This again emphasizes the ability of benzoic acid to induce a high level of defectivity to the UiO-66 framework, even when used at relatively low concentrations. If we consider that the Reo-Benz model misses 25% of the clusters (three Zr-bricks instead of four in the unit cell), the 50Benz sample (the most defective material) is missing 19.5% of the clusters.

Nitrogen sorption measurements were used to assess the porosity of all the UiO-66 samples. All the experimentally obtained isotherms are presented in the right plot of Figure 6, while those simulated from the "Ideal" and defective "Reo-Benz" UiO-66 structural models (see Figure 1) are shown in the left plot for comparison. Starting with the simulated isotherms, one can clearly see that the nitrogen uptake capacity of the "Reo-Benz" model (and thus, porosity) is significantly higher than that of ideal UiO-66. This essentially proves that increasing the concentration of missing cluster defects terminated by benzoate ligands should result in an increasingly porous material.

With this in mind, let us turn our attention to the experimentally obtained isotherms shown in the right plot of Figure 6. Before delving into the trends, we feel it is noteworthy to comment on the contour (profile) of the isotherms. For example, the isotherm obtained on the reference UiO-66 sample (Ref.) has a textbook type I profile, featuring a well-defined knee and perfectly flat plateau at higher relative pressures, emphasizing the uniformity of the sample's micropores. On the other hand, the isotherms obtained on the rest of the samples feature less-well-defined knees and plateaus, as is expected for defective UiO-66 materials with a broader distribution of pore sizes. Nevertheless, these cavities do not appear to enter into the mesoporous size range, as there is no evidence of hysteresis in any of the isotherms, the adsorption and desorption branches of which are perfectly superimposed over the full pressure range.
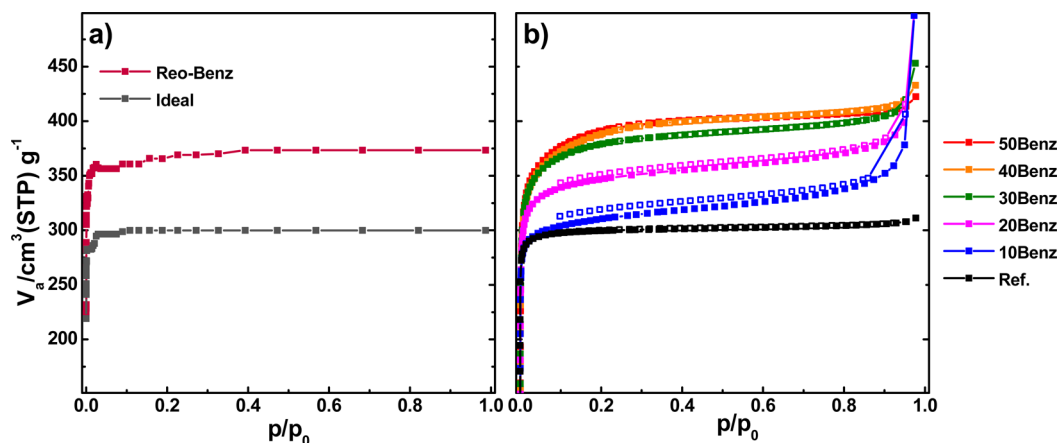
Figure 6. Simulated and experimental nitrogen adsorption isotherms obtained on all UiO-66 samples at 77 K. (a) Simulated isotherms for the Ideal (dark gray) and Reo-Benz (dark red) models. (b) Experimental isotherms; adsorption is depicted by filled squares and desorption by open squares. The same y-scale is applied to both plots.

Of greater relevance to this work is the clear trend that emerges when comparing the nitrogen uptake capacity (and thus, defectivity) of the samples. As one can see, the uptake capacity of the materials systematically increases as the amount of benzoic acid used in the synthesis was increased, eventually plateauing for the last two samples in the series (40Benz and 50Benz). This trend in porosity is quantitatively confirmed by Figure 7, in which the BET areas of the samples (calculated by
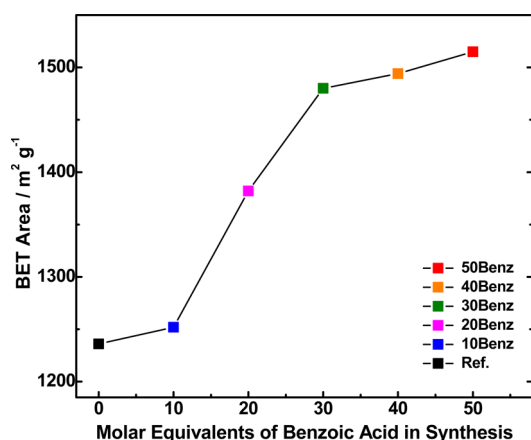
Figure 7. BET areas of the six UiO-66 samples (see also Table 2) plotted against the molar equivalents of modulator (benzoic acid) used in their synthesis.

the method outlined in section 5 of the Supporting Information; see Table 2 for numerical data) are plotted against the molar equivalents of benzoic acid added to their syntheses.

Finally, it is of interest to compare the simulated and experimental data to contextualize our results. For example, one can clearly see that the qualitative (isotherm contour) and quantitative (nitrogen uptake capacity, BET areas) data obtained on the reference material (Ref.) matches very closely with that simulated from the Ideal UiO-66 model, strongly suggesting that the sample is indeed close to defect-free. On the other hand, the data obtained on the three most defective samples (30Benz, 40Benz, and 50Benz) is similar to that simulated from the Reo-Benz model, suggesting that the three samples are extremely defective, which is an especially striking

revelation when one considers that the Reo-Benz model represents an extreme case in which one-quarter of the clusters are missing from the UiO-66 framework.

As was the case for the equivalent plots in previous work,[37] the trends observed in Figures 3, 5, and 7 appear to be qualitatively similar, prompting us to explore the relationship between the data plotted therein, $\mathrm{Rel(I)_{BP}}$, $\frac{n_{\mathrm{mod.}}}{n_{\mathrm{BDC}}}$, and BET area). To this end, we plotted the $\mathrm{Rel(I)_{BP}}$ values against the $\frac{n_{\mathrm{mod.}}}{n_{\mathrm{BDC}}}$ and BET area values of the samples (see Table 2 for numerical data), with the results shown in Figure 8.

As one can see from the fitted straight lines and R^2 values of the figure, the data is very well correlated. This makes sense when one considers that all three parameters are all in some way correlated with the concentration of defects in the UiO-66 framework, further validating their branding as "defectivity descriptors" in our previous work.[37] As also mentioned in said previous work, only one of the defectivity descriptors [the relative intensity of the broad peak, $\mathrm{Rel(I)_{BP}}$] is exclusively associated with one type of defect (missing-cluster defects). The fact that the other two descriptors are linearly correlated with $\mathrm{Rel(I)_{BP}}$ is thus a strong indication that missing-cluster defects (terminated by monocarboxylate ligands, mostly benzoate in these samples) are the predominant defect in the samples under investigation herein. This conclusion is further backed by the similarity between the nitrogen adsorption isotherms obtained on the most defective samples and the isotherm simulated from Reo-Benz, a highly defective UiO-66 structural model in which a quarter of the clusters are missing and compensated by benzoate ligands (see Figure 6 for isotherms and Figure 1 for the structural model).

While the combined evidence from these results points strongly toward the predominance of Reo-Benz-type defects in the samples under investigation herein, the individual methods each detect said defects in a rather indirect manner. We therefore speculate that some of the MOF community may be skeptical of the conclusions drawn from these results (and those of our previous papers[37,49]). Thus, we employed vibrational spectroscopic techniques (FTIR, Raman, and simulations thereof) to more directly probe the short-range order of these materials.

The O−H and C−H stretching region of the transmission FTIR spectra obtained on the full set of samples after thorough
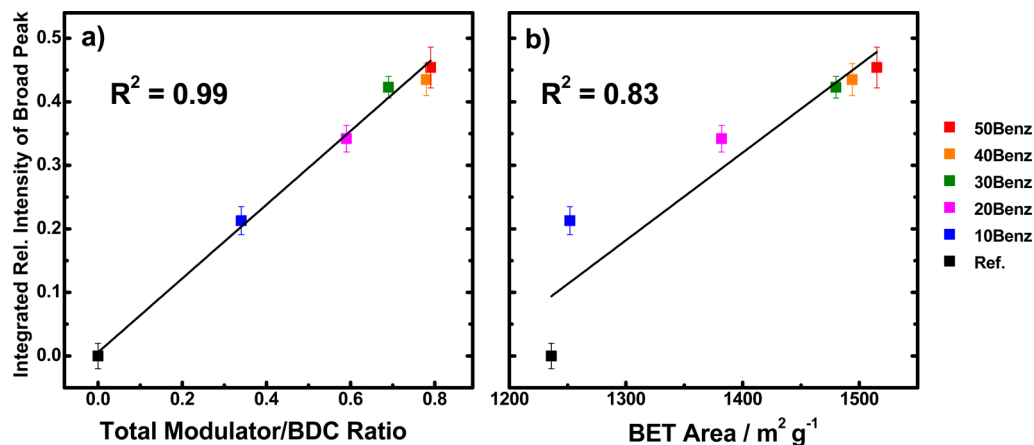
Figure 8. Graphs and linear fits obtained when the relative intensity of the PXRD broad peak [$\mathrm{Rel(I)_{BP}}$] is plotted against (a) the total modulator to BDC ratio $\left(\frac{n_{\mathrm{mod.}}}{n_{\mathrm{BDC}}}\right)$ and (b) the BET area.

activation (see Experimental Section) is reported in Figure 9a. As one can see, the spectrum obtained on the Ref. sample is
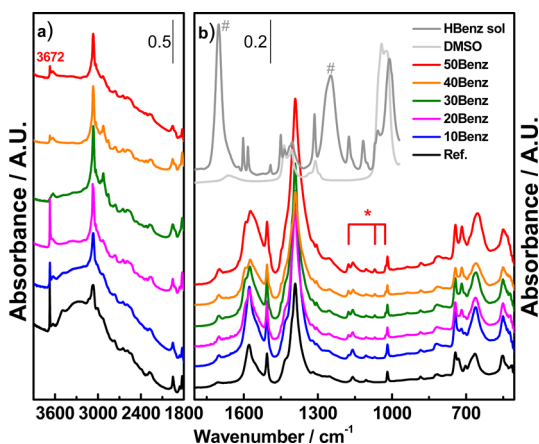

Figure 9. (a) Transmission FTIR spectra obtained for UiO-66 samples activated under dynamic vacuum for 2 h at 200 °C. (b) ATR-IR spectra obtained for the samples in air and for benzoic acid (in DMSO solution) and DMSO are also reported for comparison.

characterized by an intense and sharp band at 3672 cm^{-1}, attributed to the isolated $\mu_3(OH)$ groups on the hydroxylated $Zr_6O_4(OH)_4^{12+}$ cluster.[82,95] Its spectrum also features a broad band centered at 3250 cm^{-1}, which is due to hydrogen-bonded species. The barycenter of this band is rather low in frequency, testifying that the hydrogen bonding is rather strong. The aromatic C−H stretching region of the spectrum features a clear band at 3065 cm^{-1}, which we assign to C−H stretching modes of the BDC linkers.

Moving on to the set of samples made with benzoic acid as modulator, we observe that all the absorptions due to $\nu(OH)$ modes drastically decrease in intensity, both the hydrogen-bonded species (the broad band centered at 3250 cm^{-1}) and the isolated $\mu_3(OH)$ groups at 3672 cm^{-1} (especially in the three most defective samples, 30Benz, 40Benz, and 50Benz). This interesting observation signifies that the samples made with benzoic acid as modulator are more easily activated and dehydroxylated, indicating that they adsorb water less strongly. Indeed, the larger pores of these defective samples may be expected to provide lesser dispersion forces, thus weakening their adsorptive strength for small molecules. Part b of Figure 9 compares the ATR-IR spectra obtained on the full set of samples, which are presented together with ATR-IR spectra obtained on benzoic acid (in DMSO solution) and pure DMSO. The benzoic acid spectrum is included to determine whether the benzoate detected in the samples (see ^{1}H NMR results in Figure 4) can simply be attributed to free benzoic acid molecules in the MOF pores. However, it is clear that this is not the case since benzoic acid's most intense signals at 1700 and 1250 cm^{-1} [due to $\nu(C=O)$ and $\nu(C-O)$, respectively, highlighted by the hashes in Figure 9b] are only very faintly visible in the spectra obtained on the UiO-66 samples and do not have a clear relationship with the amount of benzoic acid used in their syntheses, as more clearly shown in Figure S2. Instead, they feature bands at 1580 and 1394 cm^{-1}, due to the $\nu_{asym}(OCO)$ and $\nu_{sym}(OCO)$ modes of carboxylate groups, respectively. One may have expected to see a trend in which the intensity of these bands follows the amount of benzoic acid used in the synthesis, but this is not the case, since the carboxylate groups are not unique to benzoate (they are also

present in the linker and formate ligands). However, a trend is clearly observed in the intensity of the weak signals falling at 1178, 1070, and 1025 cm^{-1} (each highlighted by the asterisk in Figure 9b), eventually plateauing in the spectra obtained on 40Benz and 50Benz. An enlarged view of this spectral range is reported in the Supporting Information (Figure S1). This trend is very similar to that of the defect descriptors discussed earlier, strongly suggesting that these bands are associated with the presence of defect-compensating benzoate moieties in the UiO-66 framework..

The Raman spectra obtained on the full set of samples (after thorough activation; see the Experimental Section) are presented in Figure 10, together with those recorded on solid benzoic acid, benzoic acid in DMSO solution, and pure DMSO.
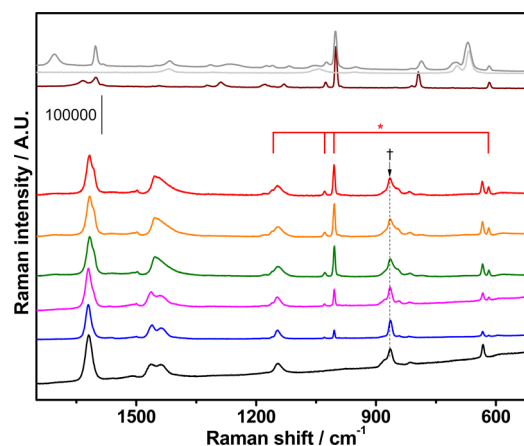
Figure 10. Raman spectra obtained on the full set of samples (activated under dynamic vacuum for 2 h at 200 °C), solid benzoic acid, benzoic acid in DMSO solution, and DMSO. The UiO-66 spectra were normalized to the intensity of the band at 866 cm^{-1} (emphasized with a dagger in the figure). Key: UiO-66-Ref. (black), 10Benz (blue), 20Benz (magenta), 30Benz (green), 40Benz (orange), 50Benz (red), solid benzoic acid (brown), benzoic acid in DMSO (gray), and DMSO (light gray).

As one can see, the Raman spectra of these materials feature many fewer bands than their FTIR counterpart, allowing for an easier identification of specific fingerprints ascribable to the presence of the benzoate ligands. Spectra obtained on benzoic acid (both as a pure solid and as a DMSO solution) have again been included for comparison to determine whether any free benzoic acid (evidenced in previous studies[77]) is present in the MOF pores. To this end, it is clear that benzoic acid was completely removed by washing since key bands [such as the $\nu(C=O)$ at 1705 cm^{-1} and $\nu(C-O)$ at 1260 cm^{-1}, among others] are completely absent from the UiO-66 spectra, as more clearly shown in Figure S2. Conversely, new bands (highlighted with an asterisk in the figure) appear at 1161 (shouldering the band at 1147 cm^{-1}), 1029, 1005, and 618 cm^{-1} in the spectra obtained on the benzoic acid-modulated UiO-66 samples, systematically increasing in intensity as the amount of benzoic acid used in the synthesis was increased. Much like the defectivity descriptors discussed throughout this work, the intensity of these bands reaches a plateau in the spectra obtained for 30Benz, 40Benz, and 50Benz, strongly suggesting that these new bands are associated with the presence of defect-compensating benzoate moieties in the UiO-66 framework.
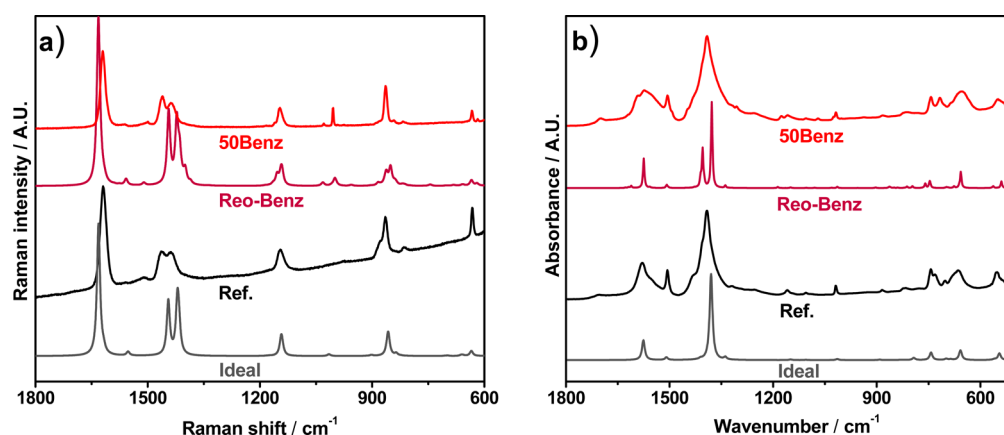
Figure 11. Comparison between simulated (dark gray and dark red) and experimental (black and red) spectra of Ref. (black) and 50Benz MOFs (red) samples with Ideal (dark gray) and Reo-Benz (dark red) models by the means of Raman (a) and IR (b) spectroscopies.

Table 3. Assignment of a Selection of Experimental and Calculated Vibrational Modes Compared for the Perfect "Ideal" and Defective "Reo-Benz" Models[a]

experimental		computed		
IR	Raman	IR	Raman	description of the mode
3672	not visible	3812	3812	OH stretching of isolated hydroxyls
3065	not active	3181, 3176	not active	CH stretching in terephthalate and benzoate
3030	not visible	3146, 3139	3146, 3139	CH stretching in benzoate
1700	1705	not calcd	not calcd	C=O stretching of benzoic acid
1580	not visible	1575	1575	OCO asymmetric stretching in carboxylate
not active	1620	not active	1632	C=C stretching of aromatic rings
not detectable	1452, 1434	1445, 1422	1445, 1422	OCO symmetric stretching in carboxylate in-phase
1394	not active	1378	not active	OCO symmetric stretching in carboxylate out-of-phase
1252	1260	not calcd	not calcd	C–O stretching of benzoic acid
1178	not active	1187	not active	in-plane CH bending in benzoates
1158	not active	1150	not active	in-plane CH bending in terephthalates and benzoates
not active	1161	not active	1165	in plane CCH bending in benzoates
not active	1147	not active	1154	terephthalates rings breathing + benzoate rings deformation
1070	not active	1080	not active	in-plane CCH bending in benzoates
1025	1029	1031	1031	benzene ring deformation in benzoates
1019	not active	1014	not active	benzene ring deformation in terephthalates
not active	1005	not active	1001	benzene ring deformation in benzoates
not active	633	not active	634	benzene ring deformation in terephthalates
not active	618	not active	619	benzene ring deformation in benzoates

[a]A scaling factor of 0.98 has been adopted in order to correct for the DFT overestimation issue.

In order to assign all these spectroscopic features, a parallel computational study on the perfect "Ideal" UiO-66 framework and on the Reo-Benz defective counterpart (see the Experimental Section for the details) has been conducted. Parts a and b of Figure 11 compare the experimental data obtained in case of 50Benz UiO-66 sample with the computed ones. Thanks to the possibility to animate each vibrational frequency, the assignments of major bands was possible. Table 3 summarizes the most relevant vibrational features with the corresponding assignment based on the animations visualized for both Raman and IR computed spectra.

At least four signals of the Raman spectra can be unambiguously assigned to the presence of modeled defects: the modes falling at 1029, 1005, and 618 cm^{-1}, present only in the defective samples, are due to the deformation of the benzene rings belonging to benzoate moieties (vibrational modes that are prohibited for symmetry in terephthalates). The 1161 cm^{-1} signal is similarly assigned to a CH bending mode

involving the proton in the para position with respect to the carboxylate in benzoates.

In the IR spectra three very weak signals falling at 1178, 1070, and 1025 cm^{-1} (shoulder) are ascribed in the same way to ring deformations and CH bending modes.

The computed intensity of all these signals with respect to the measured ones is slightly higher, as the Reo-Benz model has been constructed with a molar ratio between benzoates and terephthalates of 1:1, whereas liquid NMR measurements (see Table 2 and Table S2, Supporting Information) have found only a molar ratio of 0.78:1 for the 50Benz sample. It should be noticed that, as the broadening of the computed spectral signals is arbitrarily set to 5 cm^{-1}, only the integrated intensity should be taken into account.

The ν(C–H) region (reported only for experimental infrared spectroscopy in Figure 9a), which shows two different signals belonging to terephthalates and benzoates (falling respectively at 3065 and 3030 cm^{-1}), is again nicely modeled by the DFT calculations.

4. CONCLUSIONS

A systematic and detailed study about the synthetic insertion of missing-cluster defects (via benzoic acid additions) inside the UiO-66 framework has been reported through the present work, together with their characterization with a selection of techniques. While the long-range crystalline order of the original framework has been preserved, as demonstrated by the PXRD patterns, tiny nanoregions where defects order themselves were identified by the growth of a broad symmetry-prohibited diffraction peak, the intensity of which is strongly correlated with the number of introduced defects.

The true concentration of Reo-Benz defects has been accurately measured with dissolution liquid ^{1}H/NMR spectroscopy: the outcome reveals that even massive excesses of benzoic acid during synthesis (up to 50 equiv in the 50Benz sample) are only able to insert about 0.78 benzoic moieties per terephthalic ligand: this number is likely to be a plateau, as also 30Benz and 40Benz samples almost reached this value.

Coming to N_2 physisorption measurements, we noticed that defectivity is able to effectively increase the accessible surface area inside the framework by about 30% with respect to the reference sample with a change in the shape of the isotherm, which probably points out differences in the dimensions of the micropores now accessible thanks to the presence of defects. Vibrational spectroscopy (IR and Raman) measurements gave a beautiful set of spectra with a series of signals for which the relative intensity is growing with the concentration of defects; the identity of every vibrational band has been fully assigned with ab initio DFT calculations and the graphical analysis of the vibrational modes. The effectiveness of the constructed atomistic models, representative of both ideal and defective structures, is confirmed by both isotherm simulation and simulated IR and Raman vibrational spectra, which are in nice agreement with experimental results. Nevertheless, in situ IR spectroscopy of vacuum-treated samples pointed out that defective samples are more hydrophobic than their ideal counterpart, a result that is in agreement with the nonpolar nature of benzoate moieties.

This work also demonstrates that these techniques can be used as a "tool-box" to probe the presence and the concentration of dangling benzoate moieties inside the MOF; this approach could potentially be extended to different chemical species (i.e., other monodentate ligands) if they also present a well-defined spectroscopic fingerprint.

Empowered by these results, we presented in the present paper strong evidence of the possibility to include benzoate-decorated defects inside the UiO-66 framework and to specifically characterize them. This "defect-engineering" approach is able to increase the sorptive performance of this material by a significant degree, as discussed in the Introduction, and can be used to tune the properties of these materials for specific applications.

ASSOCIATED CONTENT

ⓢ Supporting Information

The Supporting Information is available free of charge on the ACS Publications website at DOI: 10.1021/acs.jpcc.7b00483.

> Quantitative data extracted from PXRD and ^{1}H/NMR measurements; comparison between vibrational spectra of MOFs and benzoic acid; detailed description of the method used for calculating the relative intensity of the broad PXRD peak, the BET area, and the molar ratios between linker and modulator from ^{1}H/NMR data (PDF)

AUTHOR INFORMATION

Corresponding Author
*E-mail: silvia.bordiga@unito.it.
ORCID ⓘ
Carlo Lamberti: 0000-0001-8004-2312
Silvia Bordiga: 0000-0003-2371-4156
Notes
The authors declare no competing financial interest.

REFERENCES

(1) Furukawa, H.; Cordova, K. E.; O'Keeffe, M.; Yaghi, O. M. The Chemistry and Applications of Metal-Organic Frameworks. *Science* **2013**, *341*, 1230444.

(2) Kaskel, S. The Chemistry of Metal−Organic Frameworks: Synthesis. In *Characterization, and Applications*; Kaskel, S., Ed.; John Wiley & Sons: Weinheim, 2016.

(3) Sumida, K.; Rogow, D. L.; Mason, J. A.; McDonald, T. M.; Bloch, E. D.; Herm, Z. R.; Bae, T.-H. H.; Long, J. R. Carbon Dioxide Capture in Metal-Organic Frameworks. *Chem. Rev.* **2012**, *112*, 724−781.

(4) Corma, A.; García, H.; Llabrés i Xamena, F. X. Engineering Metal Organic Frameworks for Heterogeneous Catalysis. *Chem. Rev.* **2010**, *110*, 4606−4655.

(5) Kaye, S. S.; Dailly, A.; Yaghi, O. M.; Long, J. R. Impact of Preparation and Handling on the Hydrogen Storage Properties of $Zn_4O(1,4\text{-benzenedicarboxylate})_3$ (MOF-5). *J. Am. Chem. Soc.* **2007**, *129*, 14176−14177.

(6) Tan, K.; Nijem, N.; Canepa, P.; Gong, Q.; Li, J.; Thonhauser, T.; Chabal, Y. J. Stability and Hydrolyzation of Metal Organic Frameworks with Paddle-Wheel SBUs upon Hydration. *Chem. Mater.* **2012**, *24*, 3153−3167.

(7) Saha, D.; Deng, S. Structural Stability of Metal Organic Framework MOF-177. *J. Phys. Chem. Lett.* **2010**, *1*, 73−78.

(8) Lu, P.; Wu, Y.; Kang, H.; Wei, H.; Liu, H.; Fang, M. What Can pKa and NBO Charges of the Ligands Tell Us about the Water and Thermal Stability of Metal Organic Frameworks? *J. Mater. Chem. A* **2014**, *2*, 16250−16267.

(9) Bosch, M.; Zhang, M.; Zhou, H.-C. Increasing the Stability of Metal-Organic Frameworks. *Adv. Chem.* **2014**, *2014*, 1−8.

(10) Kalidindi, S. B.; Nayak, S.; Briggs, M. E.; Jansat, S.; Katsoulidis, A. P.; Miller, G. J.; Warren, J. E.; Antypov, D.; Corà, F.; Slater, B.; et al. Chemical and Structural Stability of Zirconium-Based Metal-Organic Frameworks with Large Three-Dimensional Pores by Linker Engineering. *Angew. Chem., Int. Ed.* **2015**, *54*, 221−226.

(11) Wang, B.; Lv, X. L.; Feng, D.; Xie, L. H.; Zhang, J.; Li, M.; Xie, Y.; Li, J. R.; Zhou, H. C. Highly Stable Zr(IV)-Based Metal-Organic Frameworks for the Detection and Removal of Antibiotics and Organic Explosives in Water. *J. Am. Chem. Soc.* **2016**, *138*, 6204−6216.

(12) Cavka, J. H.; Jakobsen, S.; Olsbye, U.; Guillou, N.; Lamberti, C.; Bordiga, S.; Lillerud, K. P. A New Zirconium Inorganic Building Brick Forming Metal Organic Frameworks with Exceptional Stability. *J. Am. Chem. Soc.* **2008**, *130*, 13850−13851.

(13) Schaate, A.; Roy, P.; Preuße, T.; Lohmeier, S. J.; Godt, A.; Behrens, P. Porous Interpenetrated Zirconium-Organic Frameworks (PIZOFs): A Chemically Versatile Family of Metal-Organic Frameworks. *Chem. - Eur. J.* **2011**, *17*, 9320−9325.

(14) Wang, R.; Wang, Z.; Xu, Y.; Dai, F.; Zhang, L.; Sun, D. Porous Zirconium Metal−Organic Framework Constructed from 2D → 3D Interpenetration Based on a 3,6-Connected kgd Net. *Inorg. Chem.* **2014**, *53*, 7086−7088.

(15) Ma, J.; Wong-Foy, A. G.; Matzger, A. J. The Role of Modulators in Controlling Layer Spacings in a Tritopic Linker Based Zirconium 2D Microporous Coordination Polymer. *Inorg. Chem.* **2015**, *54*, 4591−4593.

(16) Kandiah, M.; Nilsen, M. H.; Usseglio, S.; Jakobsen, S.; Olsbye, U.; Tilset, M.; Larabi, C.; Quadrelli, E. A.; Bonino, F.; Lillerud, K. P. Synthesis and Stability of Tagged UiO-66 Zr-MOFs. *Chem. Mater.* **2010**, *22*, 6632−6640.

(17) Cavka, J. H.; Grande, C. A.; Mondino, G.; Blom, R. High Pressure Adsorption of CO_2 and CH_4 on Zr-MOFs. *Ind. Eng. Chem. Res.* **2014**, *53*, 15500−15507.

(18) Øien-ØDegaard, S.; Bouchevreau, B.; Hylland, K.; Wu, L.; Blom, R.; Grande, C.; Olsbye, U.; Tilset, M.; Lillerud, K. P. UiO-67-Type Metal-Organic Frameworks with Enhanced Water Stability and Methane Adsorption Capacity. *Inorg. Chem.* **2016**, *55*, 1986−1991.

(19) Yee, K. K.; Reimer, N.; Liu, J.; Cheng, S. Y.; Yiu, S. M.; Weber, J.; Stock, N.; Xu, Z. Effective Mercury Sorption by Thiol-Laced Metal-Organic Frameworks: In Strong Acid and the Vapor Phase. *J. Am. Chem. Soc.* **2013**, *135*, 7795−7798.

(20) Pullen, S.; Fei, H.; Orthaber, A.; Cohen, S. M.; Ott, S. Enhanced Photochemical Hydrogen Production by a Molecular Diiron Catalyst Incorporated into a Metal-Organic Framework. *J. Am. Chem. Soc.* **2013**, *135*, 16997−17003.

(21) Biswas, S.; Zhang, J.; Li, Z.; Liu, Y.-Y.; Grzywa, M.; Sun, L.; Volkmer, D.; Van Der Voort, P. Enhanced Selectivity of CO_2 over CH_4 in Sulphonate-, Carboxylate- and Iodo-Functionalized UiO-66 Frameworks. *Dalton Trans.* **2013**, *42*, 4730.

(22) Huang, Y.; Qin, W.; Li, Z.; Li, Y. Enhanced Stability and CO_2 Affinity of a UiO-66 Type Metal-Organic Framework Decorated with Dimethyl Groups. *Dalton Trans.* **2012**, *41*, 9283−9285.

(23) Biswas, S.; Van Der Voort, P. A General Strategy for the Synthesis of Functionalised UiO-66 Frameworks: Characterisation, Stability and CO_2 Adsorption Properties. *Eur. J. Inorg. Chem.* **2013**, *2013*, 2154−2160.

(24) Lin Foo, M.; Horike, S.; Fukushima, T.; Hijikata, Y.; Kubota, Y.; Takata, M.; Kitagawa, S. Ligand-Based Solid Solution Approach to Stabilisation of Sulphonic Acid Groups in Porous Coordination Polymer $Zr_6O_4(OH)_4(BDC)_6$ (UiO-66). *Dalton Trans.* **2012**, *41*, 13791−13794.

(25) Fei, H.; Cohen, S. M. Metalation of a Thiocatechol-Functionalized Zr(IV)-Based Metal-Organic Framework for Selective C-H Functionalization. *J. Am. Chem. Soc.* **2015**, *137*, 2191−2194.

(26) Jasuja, H.; Zang, J.; Sholl, D. S.; Walton, K. S. Rational Tuning of Water Vapor and CO_2 Adsorption in Highly Stable Zr-Based MOFs. *J. Phys. Chem. C* **2012**, *116*, 23526−23532.

(27) Fei, H.; Shin, J.; Meng, Y. S.; Adelhardt, M.; Sutter, J.; Meyer, K.; Cohen, S. M. Reusable Oxidation Catalysis Using Metal-Monocatecholato Species in a Robust Metal-Organic Framework. *J. Am. Chem. Soc.* **2014**, *136*, 4965−4973.

(28) Nickerl, G.; Senkovska, I.; Kaskel, S. Tetrazine Functionalized Zirconium MOF as Optical Sensor for Oxidizing Gases. *Chem. Commun.* **2015**, *51*, 2280−2282.

(29) Yang, Q.; Vaesen, S.; Ragon, F.; Wiersum, A. D.; Wu, D.; Lago, A.; Devic, T.; Martineau, C.; Taulelle, F.; Llewellyn, P. L.; et al. A Water Stable Metal-Organic Framework with Optimal Features for CO_2 Capture. *Angew. Chem., Int. Ed.* **2013**, *52*, 10316−10320.

(30) Xydias, P.; Spanopoulos, I.; Klontzas, E.; Froudakis, G. E.; Trikalitis, P. N. Drastic Enhancement of the CO_2 Adsorption Properties in Sulfone-Functionalized Zr- and Hf-UiO-67 MOFs with Hierarchical Mesopores. *Inorg. Chem.* **2014**, *53*, 679−681.

(31) Chavan, S.; Vitillo, J. G.; Uddin, M. J.; Bonino, F.; Lamberti, C.; Groppo, E.; Lillerud, K.-P.; Bordiga, S. Functionalization of UiO-66 Metal−Organic Framework and Highly Cross-Linked Polystyrene with $Cr(CO)_3$: In Situ Formation, Stability, and Photoreactivity. *Chem. Mater.* **2010**, *22*, 4602−4611.

(32) Øien, S.; Agostini, G.; Svelle, S.; Borfecchia, E.; Lomachenko, K. A.; Mino, L.; Gallo, E.; Bordiga, S.; Olsbye, U.; Lillerud, K. P. Probing Reactive Platinum Sites in UiO-67 Zirconium Metal−Organic Frameworks. *Chem. Mater.* **2015**, *27*, 1042−1056.

(33) Ragon, F.; Campo, B.; Yang, Q.; Martineau, C.; Wiersum, A. D.; Lago, A.; Guillerm, V.; Hemsley, C.; Eubank, J. F.; Vishnuvarthan, M.; et al. Acid-Functionalized UiO-66(Zr) MOFs and Their Evolution after Intra-Framework Cross-Linking: Structural Features and Sorption Properties. *J. Mater. Chem. A* **2015**, *3*, 3294−3309.

(34) Chavan, S. M.; Shearer, G. C.; Svelle, S.; Olsbye, U.; Bonino, F.; Ethiraj, J.; Lillerud, K. P.; Bordiga, S. Synthesis and Characterization of Amine-Functionalized Mixed- Ligand Metal − Organic Frameworks of UiO-66 Topology. *Inorg. Chem.* **2014**, *53*, 9509−9515.

(35) DeCoste, J. B.; Peterson, G. W.; Jasuja, H.; Glover, T. G.; Huang, Y.; Walton, K. S. Stability and Degradation Mechanisms of Metal-Organic Frameworks Containing the $Zr_6O_4(OH)_4$ Secondary Building Unit. *J. Mater. Chem. A* **2013**, *1*, 5642−5650.

(36) Hylland, K.; Øien-Ødegaard, S.; Lillerud, K.; Tilset, M. Efficient, Scalable Syntheses of Linker Molecules for Metal-Organic Frameworks. *Synlett* **2015**, *26*, 1480−1485.

(37) Shearer, G. C.; Chavan, S.; Bordiga, S.; Svelle, S.; Olsbye, U.; Lillerud, K. P. Defect Engineering: Tuning the Porosity and Composition of the Metal-Organic Framework UiO-66 via Modulated Synthesis. *Chem. Mater.* **2016**, *28*, 3749−3761.

(38) Liang, W.; Coghlan, C. J.; Ragon, F.; Rubio-Martinez, M.; D'Alessandro, D. M.; Babarao, R. Defect Engineering of UiO-66 for CO_2 and H_2O Uptake − a Combined Experimental and Simulation Study. *Dalton Trans.* **2016**, *45*, 4496−4500.

(39) Fang, Z.; Bueken, B.; De Vos, D. E.; Fischer, R. A. Defect-Engineered Metal-Organic Frameworks. *Angew. Chem., Int. Ed.* **2015**, *54*, 7234−7254.

(40) Wu, D.; Yan, W.; Xu, H.; Zhang, E.; Li, Q. Defect Engineering of Mn-Based MOFs with Rod-Shaped Building Units by Organic Linker Fragmentation. *Inorg. Chim. Acta* **2017**, *460*, 93−98.

(41) Kozachuk, O.; Luz, I.; Llabrés i Xamena, F. X.; Noei, H.; Kauer, M.; Albada, H. B.; Bloch, E. D.; Marler, B.; Wang, Y.; Muhler, M.; et al. Multifunctional, Defect-Engineered Metal-Organic Frameworks with Ruthenium Centers: Sorption and Catalytic Properties. *Angew. Chem., Int. Ed.* **2014**, *53*, 7058−7062.

(42) Jiang, Z. R.; Wang, H.; Hu, Y.; Lu, J.; Jiang, H. L. Polar Group and Defect Engineering in a Metal-Organic Framework: Synergistic Promotion of Carbon Dioxide Sorption and Conversion. *ChemSusChem* **2015**, *8*, 878−885.

(43) DeStefano, M. R.; Islamoglu, T.; Garibay, S. J.; Hupp, J. T.; Farha, O. K. Room Temperature Synthesis of UiO-66 and the Thermal Modulation of Densities of Defect Sites. *Chem. Mater.* **2017**, *29*, 1357−1361.

(44) Dissegna, S.; Hardian, R.; Epp, K.; Kieslich, G.; Coulet, M.-V.; Llewellyn, P.; Fischer, R. A. Using Water Adsorption Measurements To Access the Chemistry of Defects in the Metal−Organic Framework UiO-66. *CrystEngComm* **2017**, in press, DOI: 10.1039/C7CE00224F.

(45) Takashima, Y.; Sato, Y.; Tsuruoka, T.; Akamatsu, K. Unusual Colorimetric Change for Alkane Solvents with a Porous Coordination Framework. *Inorg. Chem.* **2016**, *55*, 11617−11620.

(46) Cai, G.; Jiang, H.-L. A Modulator-Induced Defect-Formation Strategy to Hierarchically Porous Metal-Organic Frameworks with High Stability. *Angew. Chem.* **2017**, *129*, 578−582.

(47) Gutov, O. V.; Hevia, M. G.; Escudero-Adán, E. C.; Shafir, A. Metal-Organic Framework (MOF) Defects under Control: Insights

into the Missing Linker Sites and Their Implication in the Reactivity of Zirconium-Based Frameworks. *Inorg. Chem.* **2015**, *54*, 8396–8400.

(48) Wu, H.; Chua, Y. S.; Krungleviciute, V.; Tyagi, M.; Chen, P.; Yildirim, T.; Zhou, W. Unusual and Highly Tunable Missing-Linker Defects in Zirconium Metal-Organic Framework UiO-66 and Their Important Effects on Gas Adsorption. *J. Am. Chem. Soc.* **2013**, *135*, 10525–10532.

(49) Shearer, G. C.; Vitillo, J. G.; Bordiga, S.; Svelle, S.; Olsbye, U.; Lillerud, K. P. Functionalizing the Defects: Postsynthetic Ligand Exchange in the Metal Organic Framework UiO-66. *Chem. Mater.* **2016**, *28*, 7190–7193.

(50) Vermoortele, F.; Bueken, B.; Le Bars, G.; Van De Voorde, B.; Vandichel, M.; Houthoofd, K.; Vimont, A.; Daturi, M.; Waroquier, M.; Van Speybroeck, V.; et al. Synthesis Modulation as a Tool to Increase the Catalytic Activity of Metal-Organic Frameworks: The Unique Case of UiO-66(Zr). *J. Am. Chem. Soc.* **2013**, *135*, 11465–11468.

(51) Vandichel, M.; Hajek, J.; Vermoortele, F.; Waroquier, M.; De Vos, D. E.; Van Speybroeck, V. Active Site Engineering in UiO-66 Type Metal−organic Frameworks by Intentional Creation of Defects: A Theoretical Rationalization. *CrystEngComm* **2015**, *17*, 395–406.

(52) Cliffe, M. J.; Wan, W.; Zou, X.; Chater, P. a; Kleppe, A. K.; Tucker, M. G.; Wilhelm, H.; Funnell, N. P.; Coudert, F.-X.; Goodwin, A. L. Correlated Defect Nanoregions in a Metal-Organic Framework. *Nat. Commun.* **2014**, *5*, 4176.

(53) Taylor, J. M.; Dekura, S.; Ikeda, R.; Kitagawa, H. Defect Control to Enhance Proton Conductivity in a Metal-Organic Framework. *Chem. Mater.* **2015**, *27*, 2286–2289.

(54) Cliffe, M. J.; Hill, J. A.; Murray, C. A.; Coudert, F.-X.; Goodwin, A. L. Defect-Dependent Colossal Negative Thermal Expansion in UiO-66(Hf) Metal−organic Framework. *Phys. Chem. Chem. Phys.* **2015**, *17*, 11586–11592.

(55) Van de Voorde, B.; Stassen, I.; Bueken, B.; Vermoortele, F.; De Vos, D.; Ameloot, R.; Tan, J.-C.; Bennett, T. D. Improving the Mechanical Stability of Zirconium-Based Metal−organic Frameworks by Incorporation of Acidic Modulators. *J. Mater. Chem. A* **2015**, *3*, 1737–1742.

(56) Ren, J.; Langmi, H. W.; Musyoka, N. M.; Mathe, M.; Kang, X.; Liao, S. Tuning Defects to Facilitate Hydrogen Storage in Core-Shell MIL-101(Cr)@UiO-66(Zr) Nanocrystals. *Mater. Today Proc.* **2015**, *2*, 3964–3972.

(57) Yang, D.; Odoh, S. O.; Borycz, J.; Wang, T. C.; Farha, O. K.; Hupp, J. T.; Cramer, C. J.; Gagliardi, L.; Gates, B. C. Tuning Zr_6 Metal-Organic Framework (MOF) Nodes as Catalyst Supports: Site Densities and Electron-Donor Properties Influence Molecular Iridium Complexes as Ethylene Conversion Catalysts. *ACS Catal.* **2016**, *6*, 235–247.

(58) Li, B.; Zhu, X.; Hu, K.; Li, Y.; Feng, J.; Shi, J.; Gu, J. Defect Creation in Metal-Organic Frameworks for Rapid and Controllable Decontamination of Roxarsone from Aqueous Solution. *J. Hazard. Mater.* **2016**, *302*, 57–64.

(59) Wang, K.; Li, C.; Liang, Y.; Han, T.; Huang, H.; Yang, Q.; Liu, D.; Zhong, C. Rational Construction of Defects in a Metal-Organic Framework for Highly Efficient Adsorption and Separation of Dyes. *Chem. Eng. J.* **2016**, *289*, 486–493.

(60) Yang, D.; Bernales, V.; Islamoglu, T.; Farha, O. K.; Hupp, J. T.; Cramer, C. J.; Gagliardi, L.; Gates, B. C. Tuning the Surface Chemistry of Metal Organic Framework Nodes: Proton Topology of the Metal-Oxide-Like Zr_6 Nodes of UiO-66 and NU-1000. *J. Am. Chem. Soc.* **2016**, *138*, 15189–15196.

(61) Katz, M. J.; Brown, Z. J.; Colón, Y. J.; Siu, P. W.; Scheidt, K. A.; Snurr, R. Q.; Hupp, J. T.; Farha, O. K. A Facile Synthesis of UiO-66, UiO-67 and Their Derivatives. *Chem. Commun.* **2013**, *49*, 9449–9451.

(62) DeCoste, J. B.; Demasky, T. J.; Katz, M. J.; Farha, O. K.; Hupp, J. T. A UiO-66 Analogue with Uncoordinated Carboxylic Acids for the Broad-Spectrum Removal of Toxic Chemicals. *New J. Chem.* **2015**, *39*, 2396–2399.

(63) Song, J. Y.; Ahmed, I.; Seo, P. W.; Jhung, S. H. UiO-66-Type Metal-Organic Framework with Free Carboxylic Acid: Versatile Adsorbents via H-Bond for Both Aqueous and Nonaqueous Phases. *ACS Appl. Mater. Interfaces* **2016**, *8*, 27394–27402.

(64) Vermoortele, F.; Vandichel, M.; Van De Voorde, B.; Ameloot, R.; Waroquier, M.; Van Speybroeck, V.; De Vos, D. E. Electronic Effects of Linker Substitution on Lewis Acid Catalysis with Metal-Organic Frameworks. *Angew. Chem., Int. Ed.* **2012**, *51*, 4887–4890.

(65) Katz, M. J.; Klet, R. C.; Moon, S.-Y.; Mondloch, J. E.; Hupp, J. T.; Farha, O. K. One Step Backward Is Two Steps Forward: Enhancing the Hydrolysis Rate of UiO-66 by Decreasing [OH^-]. *ACS Catal.* **2015**, *5*, 4637–4642.

(66) Nasalevich, M.; Hendon, C.; Santaclara, J. G.; Svane, K.; van der Linden, B.; Veber, S.; Fedin, M.; van der Veen, M.; Kapteijn, F.; Walsh, A.; et al. Electronic Origins of Photocatalytic Activity in d^0 Metal Organic Frameworks. *Sci. Rep.* **2016**, *6*, 23676.

(67) Ghosh, P.; Colón, Y. J.; Snurr, R. Q. Water Adsorption in UiO-66: The Importance of Defects. *Chem. Commun.* **2014**, *50*, 11329–11331.

(68) Han, Y.; Liu, M.; Li, K.; Zuo, Y.; Wei, Y.; Xu, S.; Zhang, G.; Song, C.; Zhang, Z. C.; Guo, X. Facile Synthesis of Morphology- and Size-Controlled Zirconium Metal-Organic Framework UiO-66: The Role of Hydrofluoric Acid in Crystallization. *CrystEngComm* **2015**, *17*, 6434–6440.

(69) Gutov, O. V.; Molina, S.; Escudero-Adán, E. C.; Shafir, A. Modulation by Amino Acids: Toward Superior Control in the Synthesis of Zirconium Metal−Organic Frameworks. *Chem. - Eur. J.* **2016**, *22*, 13582–13587.

(70) Trickett, C. A.; Gagnon, K. J.; Lee, S.; Gándara, F.; Bürgi, H. B.; Yaghi, O. M. Definitive Molecular Level Characterization of Defects in UiO-66 Crystals. *Angew. Chem., Int. Ed.* **2015**, *54*, 11162–11167.

(71) Øien, S.; Wragg, D.; Reinsch, H.; Svelle, S.; Bordiga, S.; Lamberti, C.; Lillerud, K. P. Detailed Structure Analysis of Atomic Positions and Defects in Zirconium Metal-Organic Frameworks. *Cryst. Growth Des.* **2014**, *14*, 5370–5372.

(72) Ling, S.; Slater, B. Dynamic Acidity in Defective UiO-66. *Chem. Sci.* **2016**, *7*, 4706–4712.

(73) Shearer, G. C.; Chavan, S.; Ethiraj, J.; Vitillo, J. G.; Svelle, S.; Olsbye, U.; Lamberti, C.; Bordiga, S.; Lillerud, K. P. Tuned to Perfection: Ironing out the Defects in Metal-Organic Framework UiO-66. *Chem. Mater.* **2014**, *26*, 4068–4071.

(74) Thornton, A. W.; Babarao, R.; Jain, A.; Trousselet, F.; Coudert, F.-X. Defects in Metal−organic Frameworks: A Compromise between Adsorption and Stability? *Dalton Trans.* **2016**, *45*, 4352–4359.

(75) Howarth, A. J.; Liu, Y.; Hupp, J. T.; Farha, O. K. Metal−organic Frameworks for Applications in Remediation of Oxyanion/cation-Contaminated Water. *CrystEngComm* **2015**, *17*, 7245–7253.

(76) Rogge, S. M. J.; Wieme, J.; Vanduyfhuys, L.; Vandenbrande, S.; Maurin, G.; Verstraelen, T.; Waroquier, M.; Van Speybroeck, V. Thermodynamic Insight in the High-Pressure Behavior of UiO-66: Effect of Linker Defects and Linker Expansion. *Chem. Mater.* **2016**, *28*, 5721–5732.

(77) Schaate, A.; Roy, P.; Godt, A.; Lippke, J.; Waltz, F.; Wiebcke, M.; Behrens, P. Modulated Synthesis of Zr-Based Metal-Organic Frameworks: From Nano to Single Crystals. *Chem. - Eur. J.* **2011**, *17*, 6643–6651.

(78) Ragon, F.; Horcajada, P.; Chevreau, H.; Hwang, Y. K.; Lee, U. H.; Miller, S. R.; Devic, T.; Chang, J. S.; Serre, C. In Situ Energy-Dispersive X-Ray Diffraction for the Synthesis Optimization and Scale-up of the Porous Zirconium Terephthalate UiO-66. *Inorg. Chem.* **2014**, *53*, 2491–2500.

(79) Abid, H. R.; Ang, H. M.; Wang, S. Effects of Ammonium Hydroxide on the Structure and Gas Adsorption of Nanosized Zr-MOFs (UiO-66). *Nanoscale* **2012**, *4*, 3089–3094.

(80) Marshall, R. J.; Hobday, C. L.; Murphie, C. F.; Griffin, S. L.; Morrison, C. A.; Moggach, S. A.; Forgan, R. S. Amino Acids as Highly Efficient Modulators for Single Crystals of Zirconium and Hafnium Metal−organic Frameworks. *J. Mater. Chem. A* **2016**, *4*, 6955–6963.

(81) Shearer, G. C.; Forselv, S.; Chavan, S.; Bordiga, S.; Mathisen, K.; Bjorgen, M.; Svelle, S.; Lillerud, K. P. In Situ Infrared Spectroscopic and Gravimetric Characterisation of the Solvent Removal and

Dehydroxylation of the Metal Organic Frameworks UiO-66 and UiO-67. *Top. Catal.* **2013**, *56*, 770−782.

(82) Valenzano, L.; Civalleri, B.; Chavan, S.; Bordiga, S.; Nilsen, M. H.; Jakobsen, S.; Lillerud, K. P.; Lamberti, C. Disclosing the Complex Structure of UiO-66 Metal Organic Framework: A Synergic Combination of Experiment and Theory. *Chem. Mater.* **2011**, *23*, 1700−1718.

(83) Lamberti, C.; Zecchina, A.; Groppo, E.; Bordiga, S. Probing the Surfaces of Heterogeneous Catalysts by in Situ IR Spectroscopy. *Chem. Soc. Rev.* **2010**, *39*, 4951.

(84) Bordiga, S.; Lamberti, C.; Bonino, F.; Travert, A.; Thibault-Starzyk, F. Probing Zeolites by Vibrational Spectroscopies. *Chem. Soc. Rev.* **2015**, *44*, 7262−7341.

(85) O'Keeffe, M.; Peskov, M. A.; Ramsden, S. J.; Yaghi, O. M. The Reticular Chemistry Structure Resource (RCSR) Database Of, and Symbols For, Crystal Nets. *Acc. Chem. Res.* **2008**, *41*, 1782−1789.

(86) Bonino, F.; Lamberti, C.; Chavan, S. M.; Vitillo, J. G.; Bordiga, S. Characterization of MOFs. 1. Combined Vibrational and Electronic Spectroscopies. In *Metal Organic Frameworks as Heterogeneous Catalysts*; Llabrés i Xamena, F., Gascon, J., Eds.; RSC Catalysis Series; Royal Society of Chemistry: Cambridge, 2013; pp 76−142.

(87) Bonino, F.; Lamberti, C.; Bordiga, S. IR and Raman Spectroscopies Probing MOFs Structure, Defectivity, and Reactivity. In *The Chemistry of Metal−Organic Frameworks: Synthesis, Characterization, and Applications*; Kaskel, S., Ed.; John Wiley & Sons: Weinheim, 2016; pp 657−690.

(88) Bárcia, P. S.; Guimarães, D.; Mendes, P. A. P.; Silva, J. A. C.; Guillerm, V.; Chevreau, H.; Serre, C.; Rodrigues, A. E. Reverse Shape Selectivity in the Adsorption of Hexane and Xylene Isomers in MOF UiO-66. *Microporous Mesoporous Mater.* **2011**, *139*, 67−73.

(89) Dovesi, R.; Orlando, R.; Erba, A.; Zicovich-Wilson, C. M.; Civalleri, B.; Casassa, S.; Maschio, L.; Ferrabone, M.; De La Pierre, M.; D'Arco, P.; et al. CRYSTAL14: A Program for the *Ab Initio* Investigation of Crystalline Solids. *Int. J. Quantum Chem.* **2014**, *114*, 1287−1317.

(90) Becke, A. D. Density-Functional Thermochemistry. III. The Role of Exact Exchange. *J. Chem. Phys.* **1993**, *98*, 5648−5652.

(91) Lee, C.; Yang, W.; Parr, R. G. Development of the Colle-Salvetti Correlation-Energy Formula into a Functional of the Electron Density. *Phys. Rev. B: Condens. Matter Mater. Phys.* **1988**, *37*, 785−789.

(92) Pascale, F.; Zicovich-Wilson, C. M.; López Gejo, F.; Civalleri, B.; Orlando, R.; Dovesi, R. The Calculation of the Vibrational Frequencies of Crystalline Compounds and Its Implementation in the CRYSTAL Code. *J. Comput. Chem.* **2004**, *25*, 888−897.

(93) Maschio, L.; Kirtman, B.; Rérat, M.; Orlando, R.; Dovesi, R. Ab Initio Analytical Raman Intensities for Periodic Systems through a Coupled Perturbed Hartree-Fock/Kohn-Sham Method in an Atomic Orbital Basis. II. Validation and Comparison with Experiments. *J. Chem. Phys.* **2013**, *139*, 164102.

(94) Maschio, L.; Kirtman, B.; Rérat, M.; Orlando, R.; Dovesi, R. Ab Initio Analytical Raman Intensities for Periodic Systems through a Coupled Perturbed Hartree-Fock/Kohn-Sham Method in an Atomic Orbital Basis. I. Theory. *J. Chem. Phys.* **2013**, *139*, 164101.

(95) Chavan, S.; Vitillo, J. G.; Gianolio, D.; Zavorotynska, O.; Civalleri, B.; Jakobsen, S.; Nilsen, M. H.; Valenzano, L.; Lamberti, C.; Lillerud, K. P.; et al. H_2 Storage in Isostructural UiO-67 and UiO-66 MOFs. *Phys. Chem. Chem. Phys.* **2012**, *14*, 1614−1626.